J MATER SCI **41** (2006) 1089–1096

Electrical mixing laws for composites with conducting and insulating discs by impedance spectroscopy

S. WANSOM, L. Y. WOO, S. L. HOKE, T. O. MASON*
Northwestern University, Department of Materials Science and Engineering, Evanston, IL 60208, USA
E-mail: t-mason@northwestern.edu

Published online: 4 February 2006

Composites made with conducting or insulating discs (right cylinders) in a cementitious matrix were tested by AC impedance spectroscopy. The dual-arc (conducting discs) and single-arc (insulating discs) behaviors were analyzed for conductivity vs. the volume fraction of discs. The resulting mixing laws are in excellent agreement with equations derived from existing mixing laws for the semi-dilute regime, once suitably modified for differences in shape (right cylinders vs. oblate spheroids) and alignment (random vs. aligned). Deviations from random dispersion were readily detected by conductivities in *x*, *y*, and *z* directions, suggesting that AC-IS is sensitive to any anisotropy of discs orientation in such composites. These results are completely general, with potential application for composites involving disc-shaped inclusions (e.g., flakes or cracks).

1. Introduction

An understanding of the electrical structure-property relationships in fiber-reinforced composites (FRCs) is essential for controlling their electronic applications and to enable various applications, e.g., non-destructive evaluation (NDE) and structural health monitoring. Chung and coworkers have demonstrated the use of DC electrical conductivity to monitor strain and damage accumulation in FRCs under static and dynamic loading [1, 2]. This is an important first step in the development of "smart composites" with self-monitoring capabilities. A number of systems have been investigated, e.g., polymer-matrix and ceramic-matrix composites, including cement-matrix FRCs. Other work has demonstrated that AC-impedance spectroscopy (AC-IS) can similarly be employed for NDE of FRCs, including ceramic-matrix [3, 4], cement-matrix [5–9] and even polymer-matrix [10] composites. It was also shown that AC-IS can monitor damage processes in discontinuous FRCs [11, 12].

To fully correlate the changes in DC and AC electrical properties with loading and/or damage accumulation, it is important to understand the role played by cracks in the overall electrical properties. Willis employed variational principles to predict bounds and estimates for the overall thermal conductivity of a body containing aligned ellipsoidal inclusions, with penny-shaped cracks as one of the limiting cases [13]. Benveniste and Miloh used a generalized self-consistent scheme to find an exact solution for the effective thermal conductivity of cracked bodies with random or oriented elliptical cracks [14, 15]. Nan and Birringer used an effective-medium approach to determine the thermal conductivity of particulate composites with imperfect interfacial thermal contact [16]. Of particular interest is the numerical method of Kushch and Sangani, who used multipole expansion to compute the conductivity of composites with perfectly conducting oblate spheroidal discs ("anti-cracks") and perfectly insulating oblate spheroidal discs (penny-shaped cracks) [17]. We will henceforth refer to these simulations as the KS model. To the best of the authors' knowledge, these numerical calculations have yet to be confirmed experimentally.

The present work develops the mixing laws for the electrical conductivity of composites with randomly oriented cracks, based on an "intrinsic conductivity" approach (see below) in tandem with the KS model [17]. For experimental confirmation, right cylindrical discs were used to simulate cracks in composites (in place of the oblate spheroidal discs used in the KS work). Modifications were made to the KS equations to account for the different shape (right cylinders vs. oblate spheroids) and also to account for

*Author to whom all correspondence should be addressed.
0022-2461
DOI: 10.1007/s10853-005-3645-5

differences in alignment (aligned in the KS work vs. random in the present study). It should be stressed that our results should be quite general, and can be extended to other physical phenomena involving aligned or randomly oriented flat objects (discs, flakes, cracks, pores, etc.), including thermal conductivity, diffusivity, dielectric constant, magnetic permeability, etc. [17].

Cement-matrix composites were selected as the model system in the present work for several reasons. Cement-matrix composites are relatively easy to fabricate and harden relatively quickly. An added benefit is the ability to achieve a high viscosity in the pre-cast condition just prior to set, to prevent the gravitational settling of more dense inclusions like steel. This was demonstrated in prior work involving cement composites with steel ball bearing inclusions. Homogeneous specimens were successfully prepared with no evidence of gravitational settling [18]. Also, when saturated cement paste has a moderately high electrical conductivity and a high pH. The high pH environment allows passive oxides to form on conducting inclusions (e.g., steel).

The system is also unique due to the absence of a percolation threshold for electrical conductivity. Campo *et al*. [18] reported the absence of a percolation threshold with loading levels up to 42% volume fraction of steel ball bearings in the cement matrix. They reasoned that the absence of a percolation threshold was due to insulating cement particles (median size $\approx 10\ \mu$m) completely coating the much larger ball bearings, preventing direct contact between them. The same behavior is expected in the present work. It must be stressed that such behavior is limited to inclusions whose smallest dimension is large compared to the median cement particle size ($\sim$10 μm). For inclusions with one or more dimensions comparable to or less than the median cement particle size (e.g., fibers with diameter $\leq$10 μm) percolation thresholds are routinely observed [19]. According to Charlaix *et al*. [20], the percolation threshold of flat discs should be in the range $0.15 \leq \varepsilon \leq 0.3$, where $\varepsilon = nr^3$ is the dimensionless number density of discs, based upon the number of discs per unit volume (n) and their radius (r). The largest values of ε used in the present work were 0.22 and 0.25 for the conducting and insulating discs, respectively, at a volume fraction of 0.1. The use of the cement matrix is therefore adventitious to study electrical mixing law behavior without the onset of percolation.

2. Experimental procedures

A series of composites were fabricated with either conducting (copper, 19 mm diameter) or insulating (polymer, 18.6 mm diameter) right cylindrical discs. The aspect ratios (diameter divided by thickness) were 13.7 and 15.4 for the conducting and insulating discs, respectively. Type I ordinary Portland cement (OPC) was hand-mixed with water at a water-to-cement ratio of 0.4 by weight for approximately 2 min. The mixture was then mixed at medium speed in a commercial blender for 3 min to achieve homogeneity. It was allowed to set for approximately 2 h to achieve the proper viscosity to prevent settling of the discs. The discs were mixed in thoroughly by hand and the composite paste was cast into cubic polycarbonate molds (86 × 86 × 86 mm). Samples were demolded after 24 h and stored at 100% relative humidity during curing for 7 days. For each batch of cement paste, a plain cement paste sample was also made. This was used for matrix-conductivity normalization purposes (see below). The processing route was identical to that of the composite samples outlined above.

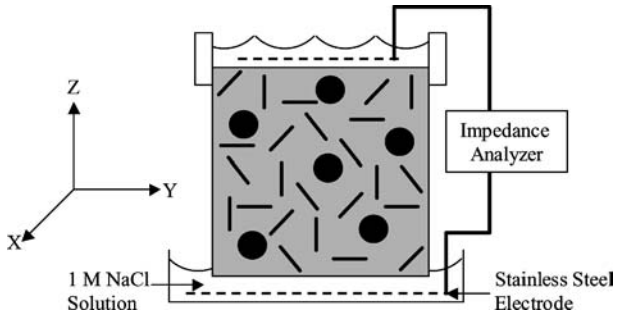

Figure 1 Experimental setup for AC-IS measurements of cement-matrix composites with either conducting or insulating right cylindrical discs.

A Solartron 1260 impedance/gain phase analyzer with Z-60 data collection software (Schlumberger, Houston, TX) was employed for the AC-IS measurements. Two-point AC-IS measurements were made at 7 days along the x, y and z directions using 1 M NaCl aqueous electrodes and stainless steel electrodes (55 × 90 × 0.5 mm). Measurements were made quickly, within 5–10 min in each direction, to limit any interdiffusion between the measurement solutions and the pore network of the composites. The experimental setup is shown in Fig. 1. The excitation amplitude was 1 V over the frequency range from 0.1 Hz to 11 MHz, with data collected at 20 steps per decade of frequency.

3. Experimental results and analysis

The measured response of AC-IS, both magnitude and phase angle, is typically represented in a Nyquist plot (negative imaginary impedance, -Im(Z), vs. real impedance, Re(Z)) with frequency increasing from right to left. The plot contains semicircles or arcs whose diameters correspond to the resistances of the different electrical components in the composite microstructure.

Fig. 2 shows a typical Nyquist plot for ordinary Portland cement (OPC) with 0.35 vol% steel fibers (2 mm length × 30 μm diameter) at 3 days of hydration [9]. The four-point DC resistance values, corrected for the different inter-electrode spacings in DC and AC measurements, are also shown. The electrode (rightmost) arc in each case is the result of a high impedance response from the external electrodes used to take measurements. The arc (for the plain OPC) or arcs (for the composite) to the left of the electrode arc, or the so-called bulk arc(s), are attributable

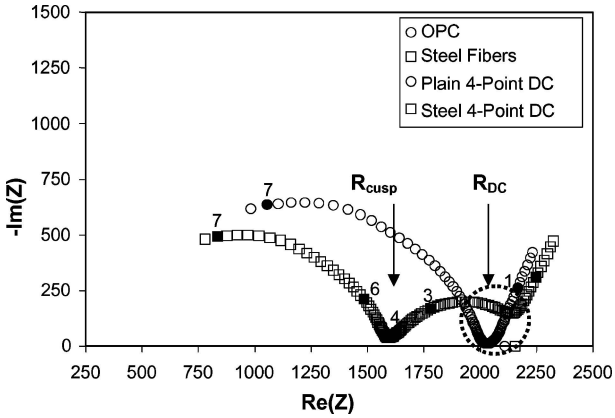

Figure 2 Typical Nyquist plots at 3 days of hydration for w/c = 0.4 OPC with and without 0.35 vol% steel fibers [9]. Four-point DC resistance values are shown on the Re(Z) axis for comparison. Darkened points indicate log (base 10) of frequency (Hz).

to the composite itself. The intersection of the electrode arc and the bulk arc at R_{DC} is in good agreement with the four-point DC measurement, as shown in each case. With a small addition of some steel fibers, the intersection and the DC resistance are relatively unaffected compared to the plain OPC. This signifies that the DC resistance is approximately that of the matrix alone and that the inclusions behave as if insulating at low frequency or DC. However, the bulk arc of the composite is now subdivided into two separate arcs, intersecting the Re(Z) axis at a lower resistance value, marked R_{cusp}. This indicates that at AC frequencies, the composite becomes much more conductive than the matrix by itself, i.e., the inclusions now behave as if conducting.

The above dual-arc behavior (as opposed to the single bulk arc of the cement matrix alone) has been observed only in composites with moderately conducting matrices and highly conducting inclusions, separated by a high impedance interface or coating [7]. Where these requirements are satisfied, such an interface may arise due to the formation of an ionic double layer (carbon fibers/OPC), a passive oxide film (steel fibers/OPC), or a Schottky barrier at the junction of two dissimilar semiconductors.

Once the above requirements are satisfied, the dual-arc behavior can be described by a frequency-switchable coating (FSC) model [7, 8]. At low frequency or DC, the high impedance interface remains intact so the inclusions actually behave as if insulating, leading to a bulk/interface cusp (and R_{DC}) that approximates that of the plain matrix. But as the frequency increases, displacement currents through the high impedance interface cause the coating to short out. Now the inclusions behave as if conducting, leading to a significantly decreased R_{cusp} value compared to R_{DC}. A comprehensive equivalent circuit model describing the impedance response of composites with insulating or conducting particles or fibers is presented elsewhere [21]. It is the presence of this high impedance coating that necessitates the use of AC conductivity to investigate the electrical behavior of composites with conducting inclusions. If such coating is not present (as is the case for composites with insulating inclusions or with conducting inclusions but no high impedance layer formation), DC conductivity is sufficient to characterize the behavior. In the present work, these two values—the cusp resistance (R_{cusp}) and the DC resistance (R_{DC})—were used to investigate electrical mixing laws for right cylindrical discs (representing cracks or flake-like inclusions) in composites.

Fig. 3a–d show some typical Nyquist plots for actual composites at the lowest ($\phi = 0.0075$) and highest ($\phi = 0.1$) disc volume fractions used in the experiments. The Nyquist plots for the x and z directions are shown for composites with conducting discs and insulating discs, respectively. (A rationale for the different responses in x vs. z directions of measurement is given below.)

Composites with conducting discs exhibit dual arc behavior, as expected, given the high impedance layer formed on the copper discs. However, there is a major convolution of the electrode and the bulk arcs, unlike the case of the fiber-reinforced composite (see Fig. 2), where the bulk-interface cusp can be readily identified. This arc convolution is due to so few interfaces being present in the disc-cement system vs. the numerous interfaces in the fiber-reinforced composite. Given such arc convolution, it is impossible to accurately extract the bulk-interface cusp (corresponding to the R_{DC} of the composite) from the Nyquist plot of the composite. Nevertheless, the cusp resistance (R_{cusp}) at higher frequencies can be combined with the R_{DC} of the plain paste sample to derive a matrix-normalized conductivity when the discs are conducting (see below).

Prior experience indicates that R_{cusp} and R_{DC} (see Fig. 2) are each reproducible to within ±5 percent, largely determined by uncertainties in electrode geometry (e.g., inter-electrode spacing). These uncertainties are reflected in the error bars of Fig. 4a and b.

Composites with insulating discs (Fig. 3a and 3b), on the other hand, exhibit only a single bulk arc similar to the plain paste sample, but shifted to higher resistance values with increased disc loading. As with conducting disc specimens, it was necessary to employ the DC conductivity of a parallel paste-only (matrix-only) specimen for normalization purposes (see below).

Assuming identical, average surroundings for each inclusion, effective medium theories have been developed to predict the effective conductivity of composites based on the geometry of a given inclusion. In the dilute limit, where the volume fraction of inclusions is sufficiently small to prevent particle-particle interactions, the effective conductivity of a composite (σ_c) containing inclusions of conductivity, σ_p, suspended in a matrix of conductivity, σ_m, is described by [23]:

$$\frac{\sigma_c}{\sigma_m} = 1 + [\sigma]_\Delta \phi + 0\phi^2, \quad \Delta \equiv \frac{\sigma_p}{\sigma_m} \qquad (1)$$

where σ_c/σ_m is the matrix-normalized conductivity of the composite and ϕ is the volume fraction of the inclusions.

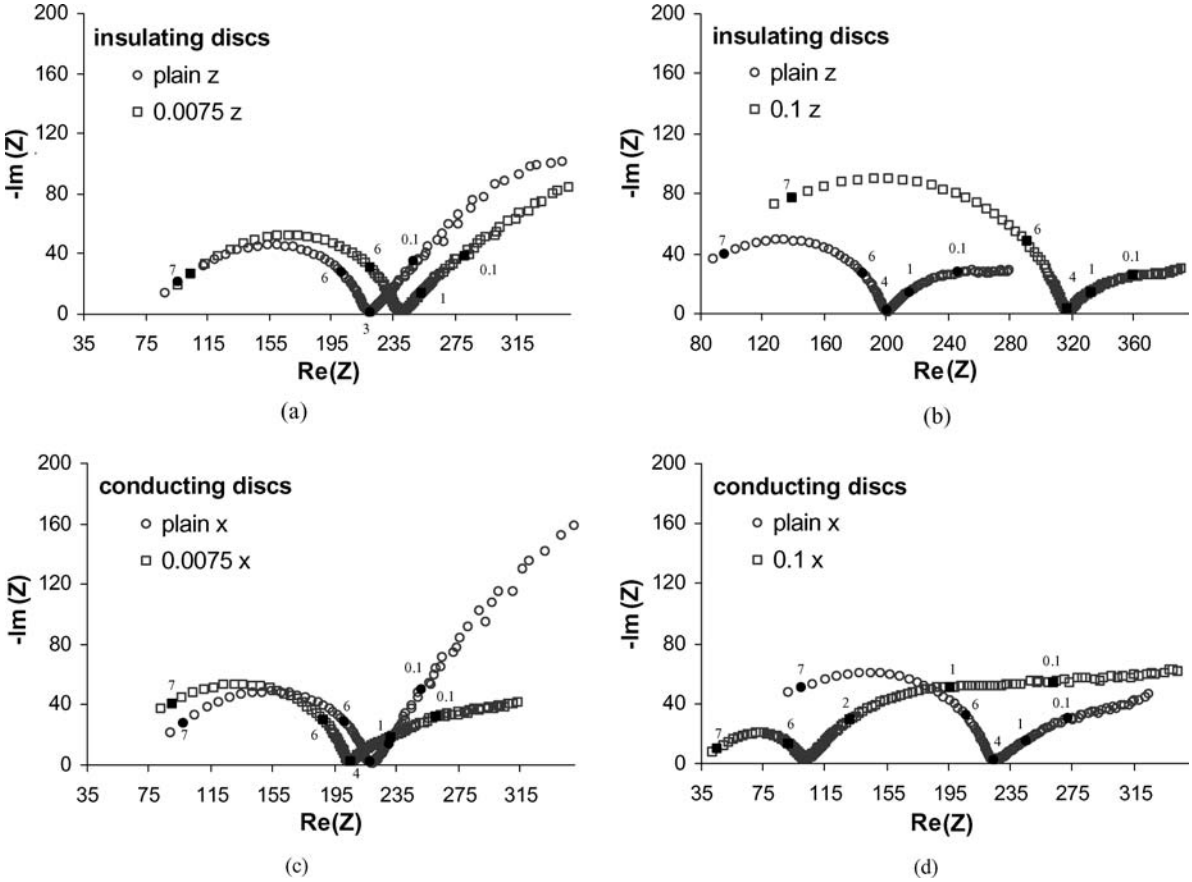

Figure 3 Typical Nyquist plots for the actual physical simulations in the present work, showing (a) the z-direction of the composite with insulating discs at $\phi = 0.0075$ (b) the z-direction of the composite with insulating discs at $\phi = 0.1$ (c) the x-direction of the composite with conducting discs at $\phi = 0.0075$ (d) the x-direction of the composite with conducting discs at $\phi = 0.1$, all of which are shown in comparison with the associated plain paste samples.

The higher order terms in ϕ are neglected for the dilute situation but will become significant outside the dilute limit. The normalized conductivity depends upon the contrast of particle vs. matrix conductivities ($\Delta = \sigma_p/\sigma_m$) and is related to the AC-IS-derived parameters through:

$$\frac{\sigma_c}{\sigma_m} = \frac{R_{DC,m}}{R_{cusp}} = 1 + [\sigma]_\infty \phi \tag{2}$$

for conducting inclusions ($\Delta = \infty$) and

$$\frac{\sigma_c}{\sigma_m} = \frac{R_{DC,m}}{R_{DC,c}} = 1 + [\sigma]_0 \phi \tag{3}$$

for insulating inclusions ($\Delta = 0$). $R_{DC,m}$ and $R_{DC,c}$ are the AC-IS-derived R_{DC} values for the matrix and the composite, respectively. The coefficient of ϕ in (1) is referred to as the "intrinsic conductivity." For example, perfectly conducting ($\Delta = \infty$) spheres have $[\sigma]_\infty = 3$, compared to $[\sigma]_0 = -3/2$ for perfectly insulating ($\Delta = 0$) spheres in the dilute limit. Outside the dilute limit, the effective conductivity of spherical particle composites is best described by the Meredith and Tobias model [18, 22]. Douglas and Garboczi calculated and compiled the intrinsic conductivities for inclusions of various shapes, including ellipsoids of revolution and right cylinders in the limiting cases when they are highly insulating ($\Delta = 0$) and highly conducting ($\Delta = \infty$) [23]. They demonstrated the important role of aspect ratio. For example, long right cylinders (fibers) can have extremely large intrinsic conductivities when conducting (e.g., see [24]), whereas flat right cylinders (discs) can have significant intrinsic conductivities whether conducting or insulating.

Beyond the intrinsic regime, only the numerical calculations of Kushch and Sangani have dealt with flat objects (e.g., cracks or flake-like inclusions) [17]. They considered an array of oblate spheroidal discs with their axes of rotation aligned parallel to the z-axis, but otherwise positioned randomly in the x-y plane. We will refer to these as z-axis aligned specimens. By curve-fitting their results vs. the number density of discs (defined above), they arrived at expressions which were valid up to $\varepsilon = 1.0$ for both conducting discs:

$$\frac{\sigma_x}{\sigma_m} = \frac{\sigma_y}{\sigma_m} = 1 + 4.71\varepsilon + 6.5\varepsilon^2, \quad \frac{\sigma_z}{\sigma_m} = 1 \tag{4}$$

and insulating discs:

$$\frac{\sigma_z}{\sigma_m} = 1 - 0.863[1 - \exp(-2.7\varepsilon)], \frac{\sigma_x}{\sigma_m} = \frac{\sigma_y}{\sigma_m} = 1 \tag{5}$$

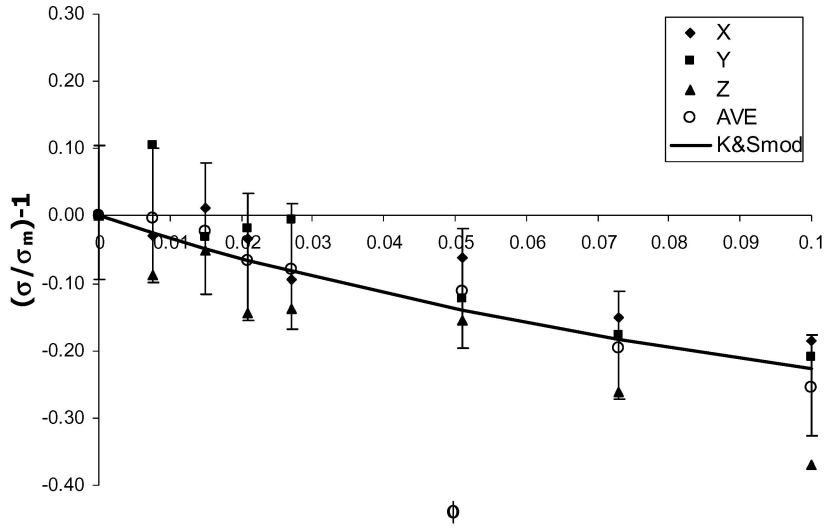

(a)

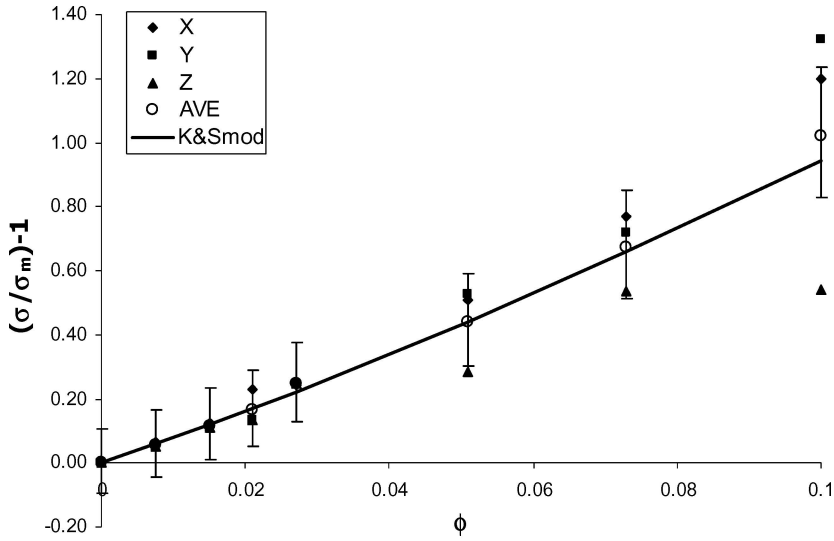

(b)

Figure 4 ($\sigma_i/\sigma_m - 1$) vs. volume fraction for (a) random insulating discs and (b) random conducting discs. The modified Kushch and Sangani equations for random orientation of right cylindrical discs are also shown. The variations of the individual data for *x*, *y*, and *z* directions before averaging are shown as well as the average value (open circle). The error bars were calculated based on the expected 5% experimental errors from geometry of the AC-IS measurements.

where the *x*, *y* and *z* subscripts denote the effective composite conductivities in each direction of measurement. The dimensionless number density ($\varepsilon = nr^3$) can be related to the disc volume fraction ϕ through

$$\varepsilon = \frac{3}{2\pi}\left(\frac{r}{t}\right)\phi \tag{6}$$

where r is the disc radius and t is its thickness. Comparison of the results show that, at a fixed volume fraction, perfectly conducting discs create a much larger change in the composite conductivity than do perfectly insulating discs. Nevertheless, flat insulating objects are the most effective geometry of inclusions to reduce the conductivity of a composite [23].

Based on Douglas and Garboczi's work on electric and magnetic polarizabilities of oblate spheroidal particles [23], equations similar to (1) can be derived in terms of ε for oblate spheroidal discs and right cylindrical discs embedded in an isotropic matrix as a function of disc orientation. The first order coefficient in ε can be converted across disc shape and/or orientation by some common factors depending on whether the discs are conducting or insulating (See Table I and details in Appendix). However, these equations hold true only in the dilute limit, which might not be the case for some volume fractions used in our experiment. The KS equations, on the other hand, extend beyond the dilute limit into the semi-dilute regime where the influence of inclusions on each other is taken into account. They are applicable up to $\varepsilon = 1.0$ which

TABLE I Normalized conductivity of oblate spheroidal discs and right cylindrical discs in the dilute limit [23]

	Oblate spheroidal discs	
Orientation	Conducting	Insulating
z-axis aligned (axis of rotation || z-axis)	$\frac{\sigma_x}{\sigma_m} = \frac{\sigma_y}{\sigma_m} = 1 + \frac{16}{3}\varepsilon$ $\frac{\sigma_z}{\sigma_m} = 1$	$\frac{\sigma_z}{\sigma_m} = 1 - \frac{8}{3}\varepsilon$ $\frac{\sigma_x}{\sigma_m} = \frac{\sigma_y}{\sigma_m} = 1$
Random	$\frac{\sigma_i}{\sigma_m} = 1 + \frac{32}{9}\varepsilon \quad i = x, y, z$	$\frac{\sigma_i}{\sigma_m} = 1 - \frac{8}{9}\varepsilon \quad i = x, y, z$
	Right cylindrical discs	
Orientation	Conducting	Insulating
z-axis aligned (axis of rotation || z-axis)	$\frac{\sigma_x}{\sigma_m} = \frac{\sigma_y}{\sigma_m} = 1 + \frac{16}{3}\varepsilon$ $\frac{\sigma_z}{\sigma_m} = 1$	$\frac{\sigma_z}{\sigma_m} = 1 - \frac{4\pi}{3}\varepsilon$ $\frac{\sigma_x}{\sigma_m} = \frac{\sigma_y}{\sigma_m} = 1$
Random	$\frac{\sigma_i}{\sigma_m} = 1 + \frac{32}{9}\varepsilon \quad i = x, y, z$	$\frac{\sigma_i}{\sigma_m} = 1 - \frac{4\pi}{9}\varepsilon \quad i = x, y, z$

corresponds to $\phi \approx 0.41$ and 0.46 for our insulating and conducting right cylindrical discs, respectively. These are well beyond the maximum volume fraction used in the present work. These expressions, when properly modified, should therefore be valid for describing the electrical mixing laws in our model composites.

Fig. 4a and b show the experimental variations of $(\sigma_i/\sigma_m - 1)$ vs. volume fraction for either type of the discs in the present work. The normalized conductivity in the i-direction σ_i/σ_m, was calculated from (2) or (3), depending on the disc type, using the AC-IS parameters measured in that particular direction. They were plotted in comparison with the KS equations, modified for the different shape and orientation of the inclusions (labeled "K&Smod"), as described in the Appendix. To account for right cylindrical discs in random orientation (as opposed to the z-axis alignment in the KS work), the coefficients of ε^n in the polynomial fits (n = 1 to 4) for the original KS data were corrected by a factor of $\pi/6$ for the insulating case and 2/3 for the conducting case (see Appendix for details). Besides the individual values of $(\sigma_i/\sigma_m - 1)$ for the x, y and z directions, the average values of $(\sigma_i/\sigma_m - 1)$ over all three directions are also shown. Due to the inability to achieve a perfectly random orientation of discs, the individual data for the three directions display some deviations from the expected trend. For both types of the discs, the z direction appears to exhibit lower conductivity than expected. Averaging over x, y and z directions, however, corrects for any unintentional alignment. As can be seen in Fig. 4a and 4b, the average values agree well with the appropriately modified KS equations. The resulting relationships (see the Appendix) can therefore be used to describe the electrical mixing law behavior in composites with random flat objects (e.g., cracks or flake-like inclusions).

The considerable variations in conductivity among the three directions as detected in Fig. 4 show that AC-IS is also sensitive to the anisotropy of inclusion distribution. This points to the potential use of these AC-IS-derived conductivities to characterize the overall orientation of the discs and thus the anisotropy of the composite structure. To explore the overall disc orientation, the effective intrinsic conductivity in each of the three directions $[\sigma]_{\Delta(i)}$ was calculated from (2) or (3) and then normalized by the sum of that same quantity over all three directions. These fractional x, y and z components of the intrinsic conductivity give the electrical contribution from the inclusions in each particular direction, from which information about the overall orientation of discs can be obtained. This is shown in the triangular plots of Fig. 5a and b for the two types of discs at various volume fractions. Due to there being very few interfaces in the samples with the lowest volume fractions of discs ($\phi = 0.0075$ and 0.015), only a miniscule variation from the plain paste conductivity is detected, leading to very large uncertainties in the intrinsic conductivity calculation. Therefore, only results from samples with larger volume fractions, i.e., with significant changes in conductivity vs. plain paste, are presented in Fig. 5. The coordinates in Fig. 5 represent $([\sigma]_{\Delta(x)}/\Sigma, [\sigma]_{\Delta(y)}/\Sigma, [\sigma]_{\Delta(z)}/\Sigma)$ where $\Sigma = [\sigma]_{\Delta(x)} + [\sigma]_{\Delta(y)} + [\sigma]_{\Delta(z)}$, therefore $[\sigma]_{\Delta(x)}/\Sigma + [\sigma]_{\Delta(y)}/\Sigma + [\sigma]_{\Delta(z)}/\Sigma$ will always be equal to 1. The open square represents the theoretical prediction for perfectly random (1/3, 1/3, 1/3) orientation of the discs. The arrows show the expected deviation from the perfectly isotropic case as a result of z-axis alignment (with the axis of rotation of the discs parallel to the z-axis of the sample), based on the intrinsic conductivity approach.

The experimental results show a shift in the direction of the z-vertex in Fig. 5a (insulating discs) and away from the z-vertex in Fig. 5b (conducting discs). Since Fig. 5a is essentially displaying negative intrinsic conductivities (insulating discs), it follows that the z-axis

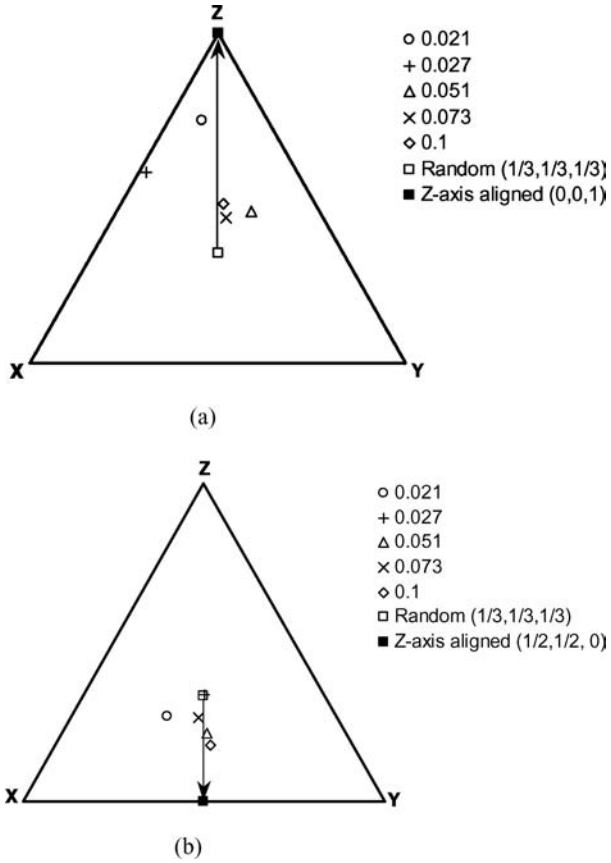

Figure 5 Triangular representation of the fractional *x*, *y* and *z* components of the intrinsic conductivity for (a) random insulating discs and (b) random conducting discs at various volume fractions. The open square at the center of the diagram represents theoretical prediction for perfectly random orientation of the discs, with arrows showing predicted shifts due to z-axis alignment of discs.

conductivities are lower than for a perfectly random distribution, in agreement with Fig. 4a. Similarly, since Fig. 5b is displaying positive intrinsic conductivities (conducting discs), it follows that the z-axis conductivities are lower than for a perfectly random distribution, in agreement with Fig. 4b. Both observations would be consistent with a greater than random fraction of discs being z-axis aligned. In the insulating state, current flow would tend to be reduced in the z-direction vs. the *x* and *y* directions. In the conducting state, current flow would tend to be enhanced in the *x* and *y* directions, with a necessary reduction in the *z*-direction. The reason for the detected *z*-axis alignment in both sets of experimental specimens is unclear. Nevertheless, the results demonstrate that AC-IS, combined with the intrinsic conductivity approach, is sensitive to any preferred alignment of disc-shaped inclusions such as cracks, flakes, etc., in composite materials.

4. Conclusions

Electrical mixing laws for composites containing insulating or conducting right cylindrical discs have been developed based on the intrinsic conductivity approach and the numerical calculations of Kushch and Sangani [17]. The averaged matrix-normalized conductivity of the model composites, obtained from AC-IS parameters, was found to be in good agreement with the KS equations, modified for the different disc shape (right cylinders in the present work vs. oblate spheroids in the KS work) and orientation (random vs. *z*-axis aligned). The modified equations can be used to describe the composite electrical behavior in the semi-dilute regime, i.e., up to $\varepsilon = \mathrm{nr}^3 = 1.0$, where n is the number of discs of radius, r, per unit volume. Furthermore, directional variations of the normalized conductivities showed that AC-IS is sensitive to the overall orientation of disc-shaped inclusions and thus the overall anisotropy of the composite. The fractional components of the intrinsic conductivity, when plotted in a triangular representation, are quite sensitive to any preferred alignment of disc-shaped inclusions. It should be possible to apply the analysis and equations developed to characterize the amount and distribution of disc-shaped inclusions, e.g., flakes or cracks, in composites. The ability to monitor the development and orientation of cracks during loading may be one useful application.

Acknowledgments

This work was supported by the National Science Foundation under grant no. DMR-00-73197 and made use of facilities of the Center for Advanced Cement-Based Materials. The authors are grateful to E. J. Garboczi and S. P. Shah for helpful discussions.

Appendix

The equations developed by Kushch and Sangani [17] for the case of z-axis aligned oblate spheroidal discs can be extended to the case of random right cylindrical discs, as in the present work.

Table I shows the normalized conductivity of oblate spheroidal discs and right cylindrical discs in the dilute limit based on Douglas and Garboczi's work on polarizabilities [23]. The non-dimensional number density ε is related to the volume fraction ϕ through Equation 6 for oblate spheroidal discs and through:

$$\varepsilon = \frac{1}{\pi}\left(\frac{r}{t}\right)\phi \tag{A1}$$

for right cylindrical discs, where *r* and *t* are the radius and thickness of the discs, respectively. Significant changes in conductivity are observed in the direction parallel to the plane of the conducting discs and perpendicular to the plane of the insulating discs.Note that for the conducting case, both oblate spheroids and right cylindrical discs yield the same behavior in terms of ε. For the insulating case, however, a factor of $\pi/2$ is involved to convert the coefficient of ε from oblate spheroids to right cylindrical

discs. Moreover, due to two electrical polarization components parallel to the plane of the discs in the conducting case, a factor of 2/3 is needed to convert from aligned to random orientation, for both oblate spheroids and right cylindrical discs. For the insulating case, only a factor of 1/3 is needed for the same purpose, since only one magnetic polarization component perpendicular to the plane of the discs is involved in conduction.

The modified KS equations plotted in Fig. 4 are:

$$\frac{\sigma_i}{\sigma_m} = 1 - 1.40\varepsilon + 2.48\varepsilon^2 - 2.60\varepsilon^3 + 1.11\varepsilon^4 \quad \text{(A2)}$$

$$\frac{\sigma_i}{\sigma_m} = 1 + 3.56\varepsilon + 3.91\varepsilon^2 - 2.07\varepsilon^3 + 2.31\varepsilon^4 \quad \text{(A3)}$$

where $i = x, y, z$ for composites containing insulating and conducting right cylindrical discs, respectively. These are obtained from polynomial fits for Kushch and Sangani's original data [17]:

$$\frac{\sigma_i}{\sigma_m} = 1 - \frac{8}{3}\varepsilon + 4.74\varepsilon^2 - 4.97\varepsilon^3 + 2.11\varepsilon^4 \quad \text{(A4)}$$

$$\frac{\sigma_i}{\sigma_m} = 1 + \frac{16}{3}\varepsilon + 5.86\varepsilon^2 - 3.10\varepsilon^3 + 3.47\varepsilon^4 \quad \text{(A5)}$$

modified by a factor of $\pi/6$ for the insulating case and 2/3 for the conducting case, respectively. Note that the original data were fitted such that the resulting equations will reduce to those derived for the intrinsic limit (Table I) when ε is very small.

References

1. D. D. L. CHUNG, *Mater. Sci. Eng.* **R 22** 1998 57.
2. D. D. L. CHUNG, in "Composite Materials for Electronic Functions," edited by M. Magini and F. H. Wohlbier, (Trans Tech Publications, Switzerland, 2000) Vol. 12 p. 58.
3. C.–A. WANG, Y. HUANG, Z. XIE, Y. LI and Z. ZHANG, *J. Am. Ceram. Soc.* **83** (2000) 2689.
4. R. GERHARDT, *Ceram. Eng. Sci. Proc.* **15** (1994) 1174.
5. P. GU, Z. XU, P. XIE and J. J. BEAUDOIN, *Cem. Concr. Res.* **23** (1993) 675.
6. S. J. FORD, J. D. SHANE and T. O. MASON, *ibid.* **28** (1998) 1737.
7. J. M. TORRENTS, T. O. MASON and E. J. GARBOCZI, *Cem. Concr. Res.* **30** (2000) 585.
8. J. M. TORRENTS, T. O. MASON, A. PELED, S. P. SHAH and E. J. GARBOCZI, *J. Mater. Sci.* **36** (2001) 4003.
9. T. O. MASON, M. A. CAMPO, A. D. HIXSON, and L. Y. WOO, *Cem. Concr. Comp.* **24** (2002) 457.
10. D. KAUSHIK, M. N. ALIAS and R. BROWN, *Corrosion* **47** 1991 859.
11. J. M. TORRENTS, T. C. EASLEY, K. T. FABER, T. O. MASON and S. P. SHAH, *J. Am. Ceram. Soc.* **84** (2001) 740.
12. A. PELED, J. M. TORRENTS, T. O. MASON, S. P. SHAH and E. J. GARBOCZI, *ACI Mat. J.* **98** (2001) 313.
13. J. R. WILLIS, *J. Mech. Phys. Solids.* **25** (1977) 185.
14. T. MILOH and Y. BENVENISTE, *J. Appl. Phys.* **63**, (1988) 789.
15. Y. BENVENISTE and T. MALOH, *ibid.* **66** (1989) 176.
16. C.-W. NAN, R. BIRRINGER, D. R. CLARKE and H. GLEITER, *J. Appl. Phys.* **81**, (1997) 6692.
17. V. I. KUSHCH and A. S. SANGANI, *Proc. R. Soc. Lond. A.* **456** (2000) 683.
18. M. A. CAMPO, L. Y. WOO, T. O. MASON and E. J. GARBOCZI, *J. Electroceram.* **9** (2002) 49.
19. P. –W. CHEN and D. D. L. CHUNG, *J. Electron. Mater.* **24** (1995) 47.
20. E. CHARLAIX, E. GUYON and N. RIVIER, *Solid State Commun.* **50** 1984 999.
21. L. Y. WOO, S. WANSOM, A. D. HIXSON, M. A. CAMPO and T. O. MASON, *J. Mater. Sci.* **38** (2003) 2265.
22. R. E. MEREDITH and C. W. TOBIAS, in "Advances in Electrochemistry and Electrochemical Engineering," edited by C. W. Tobias, (Interscience, New York, 1962) Vol. 2. p. 15.
23. J. F. DOUGLAS and E. J. GARBOCZI, in "Advances in Chemical Physics," edited by I. Prigogine and S. A. Rice, (John Wiley & Sons, 1995) Vol. XCI p. 85.
24. A. D. HIXSON, L. Y. WOO, M. A. CAMPO, T. O. MASON and E. J. GARBOCZI, *J. Electroceram* **7** 2001 189.

Received 19 March 2004
and accepted 22 June 2005